IAA-AAS-DyCoSS2-14 -07-06

ATTITUDE CONTROL OF A SPACECRAFT WITH A DOUBLE-GIMBAL VARIABLE-SPEED CONTROL MOMENT GYRO VIA LPV CONTROL THEORY

Takahiro Sasaki* **and Takashi Shimomura†**

In this paper, we analyze dynamics of a DGVSCMG(Double-Gimbal Variable-Speed Control Moment Gyro) and develop an easy-to-use LPV (Linear Parameter-Varying) model, in which we deal with 3-axis attitude control of a spacecraft equipped with a DGVSCMG. Although it is hard to consider overall stability and control performance of attitude control at the same time with conventional methods, this paper attains both of them via LPV control theory, while newly introducing an interesting PDCT (Parameter-Dependent Coordinate Transformation) as well as a virtual state variable. Through a numerical example, we demonstrated the efficiency of the proposed method to compare with a conventional method.

INTRODUCTION

Momentum Exchange Devices (MEDs) have been used to complete attitude control of spacecraft as actuators, in which they do not require fuel. In MEDs, Reaction Wheels (RWs) are often used for attitude control of satellites. However, RWs cannot respond to the demand of a high-speed attitude maneuver since they cannot provide both high-speed wheel spin rate and large torque, simply because they have only one motor. In contrast, Control Moment Gyros (CMGs) can meet this requirement since they can provide both of them. There are various types of CMGs. Single-Gimbal CMGs (SGCMGs) are one of the most common types of CMGs. They have singular points in which they cannot always output the desired torque. Several singularity avoidance methods have been proposed.[1,2,3,4] However, they tend to result in complexity of the algorithm.

Single-Gimbal Variable-Speed CMGs (SGVSCMGs) can be regarded as a kind of hybrid system which consists of a RW and an SGCMG. The extra degree of freedom (DOF) of the wheel spin rate changes can be used to avoid singularities.[5,6,7] On the other hand, Double-Gimbal CMGs can apply control torques around arbitrary axes except for singular orientations corresponding to a gimbal lock, where both inner and outer gimbals coincide with each other. To avoid such a gimbal lock, large angle motion should not be commanded in one time.[8] As a practical application, they have been used for International Space Station (ISS).

A Double-Gimbal Variable-Speed CMG (DGVSCMG) has two gimbal axes and a variable speed wheel. A DGVSCMG can generate three dimensional torques. From this advantage, we can reduce a number of actuators and weight of them. This saves an inner space of a satellite and reserves an extra space for other missions. Some works related to DGVSCMGs included in the literature.[9,10,11,12]

*Graduate Student, Department of Aerospace Engineering, Osaka Prefecture University, Japan.
†Professor, Department of Aerospace Engineering, Osaka Prefecture University, Japan.

Satellite dynamics is described by a nonlinear differential equation. Most of recent studies about attitude control have used non-linear controllers such as Lyapunov function-based controllers or Hamilton-Jacobi equation-based controllers.[13,14] With Lyapunov function-based controllers, overall stability of attitude control is always guaranteed. However, control performance is ignored in most cases. With Hamilton-Jacobi equation-based controllers, overall stability and control performance are always guaranteed. However, control performance is to be attained not in absolute optimality but in asymptotic optimality. To overcome these problems, we applied Linear Parameter-Varying (LPV) control theory[15,16] to attitude control problem.[17,18,19] To avoid difficulties coming from the nonlinearity in satellite dynamics, we modeled dynamics of spacecraft as an LPV system and applied a Gain-Scheduled (GS) controller to this model using Linear Matrix Inequalities (LMIs).

In previous study,[9] attitude control of a spacecraft with a DGVSCMG has been achieved to adopt a Lyapunov function-based controller togather with a Newton-Raphson (N-R) method. In this paper, a GS controller is designed to guarantee overall stability and achieve $\mathcal{H}_2$ performance with distinct Lyapunov solutions. By using this controller, 3-axis attitude control of a spacecraft with only one DGVSCMG has been achieved. To examine how the proposed method improves the control performance, it shall be compared with conventional methods.[13,14]

SPACECRAFT MODEL

In this paper, we deal with a spacecraft with a DGVSCMG model as shown in Figure 1. In this section, a generalized dynamics equation of a spacecraft with a DGVSCMG is presented. After that, a kinematics equation based on the quaternion is described.

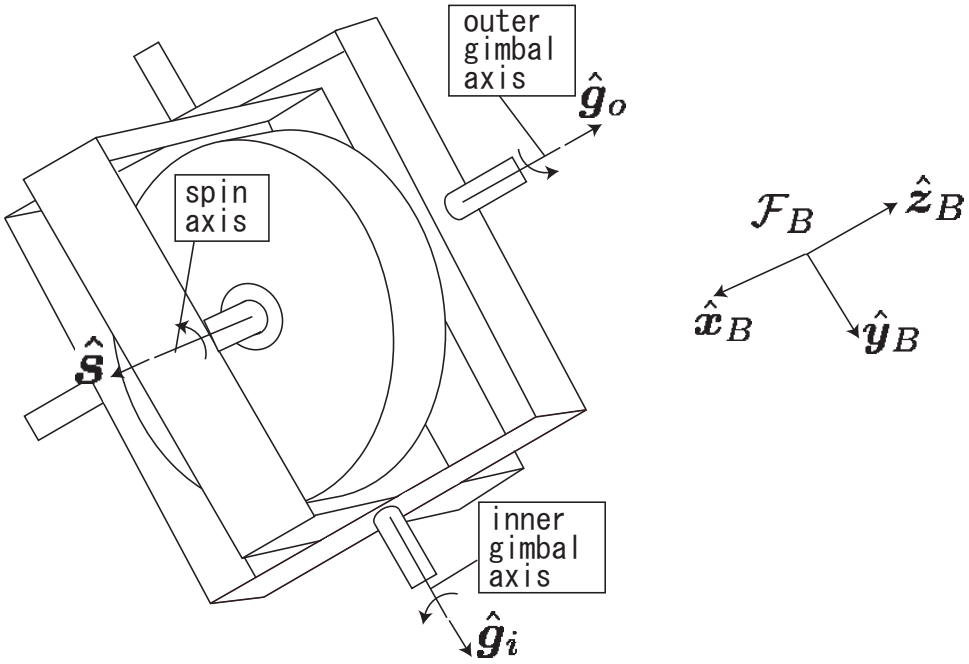

Figure 1. Double-Gimbal Variable-Speed Control Moment Gyro.

Dynamics

The spacecraft considered in this paper is assumed to be a rigid body and contains a DGVSCMG. The body fixed-frame $\mathcal{F}_B$ is represented by a set of unit vectors $\hat{\boldsymbol{x}}_B$, $\hat{\boldsymbol{y}}_B$, and $\hat{\boldsymbol{z}}_B$. Then, as in Figure 1, the unit vectors of the spin axis, the inner gimbal axis, and the outer gimbal axis are denoted by $\hat{\boldsymbol{s}}$, $\hat{\boldsymbol{g}}_i$, and $\hat{\boldsymbol{g}}_o$, respectively. The outer gimbal axis $\hat{\boldsymbol{g}}_o$ is always paraleled to $\hat{\boldsymbol{z}}_B$ of the body frame $\mathcal{F}_B$. Therefore, it is given by

$$\hat{\boldsymbol{g}}_o = \begin{bmatrix} 0 \\ 0 \\ 1 \end{bmatrix}_{\mathcal{F}_{go}} = \begin{bmatrix} 0 \\ 0 \\ 1 \end{bmatrix}_{\mathcal{F}_B}, \tag{1}$$

where $\mathcal{F}_{go}$ denotes the outer gimbal axis frame. The inner gimbal axis $\hat{\boldsymbol{g}}_i$ must rotate around the outer gimbal axis $\hat{\boldsymbol{g}}_o$. Therefore, it is given as follows:

$$\hat{\boldsymbol{g}}_i = \begin{bmatrix} \cos\delta_o & -\sin\delta_o & 0 \\ \sin\delta_o & \cos\delta_o & 0 \\ 0 & 0 & 1 \end{bmatrix} \begin{bmatrix} 0 \\ 1 \\ 0 \end{bmatrix}_{\mathcal{F}_{go}} = \begin{bmatrix} -\sin\delta_o \\ \cos\delta_o \\ 0 \end{bmatrix}_{\mathcal{F}_B}, \tag{2}$$

where δ_o is the outer gimbal angle. The spin axis $\hat{\boldsymbol{s}}$ can be expressed in the inner gimbal frame $\mathcal{F}_{gi}$ as follows:

$$\hat{\boldsymbol{s}} = \begin{bmatrix} \cos\delta_i & -\sin\delta_i & 0 \\ \sin\delta_i & \cos\delta_i & 0 \\ 0 & 0 & 1 \end{bmatrix} \begin{bmatrix} 1 \\ 0 \\ 0 \end{bmatrix}_{\mathcal{F}_s} = \begin{bmatrix} \cos\delta_i \\ \sin\delta_i \\ 0 \end{bmatrix}_{\mathcal{F}_{gi}}, \tag{3}$$

where δ_i is the inner gimbal angle and $\mathcal{F}_s$ denotes the spin axis frame. The inner gimbal frame $\mathcal{F}_{gi}$ must be corresponding to the body frame $\mathcal{F}_B$ in order to express the spin axis $\hat{\boldsymbol{s}}$ in the body frame $\mathcal{F}_B$. Therefore, it is given as follows:

$$\hat{\boldsymbol{s}} = \begin{bmatrix} \cos\delta_o & -\sin\delta_o & 0 \\ \sin\delta_o & \cos\delta_o & 0 \\ 0 & 0 & 1 \end{bmatrix} \begin{bmatrix} 1 & 0 & 0 \\ 0 & \cos\frac{\pi}{2} & \sin\frac{\pi}{2} \\ 0 & -\sin\frac{\pi}{2} & \cos\frac{\pi}{2} \end{bmatrix} \begin{bmatrix} \cos\delta_i \\ \sin\delta_i \\ 0 \end{bmatrix}_{\mathcal{F}_{gi}} \tag{4}$$

$$= \begin{bmatrix} \cos\delta_o & -\sin\delta_o & 0 \\ \sin\delta_o & \cos\delta_o & 0 \\ 0 & 0 & 1 \end{bmatrix} \begin{bmatrix} \cos\delta_i \\ 0 \\ -\sin\delta_i \end{bmatrix}_{\mathcal{F}_{go}} \tag{5}$$

$$= \begin{bmatrix} \cos\delta_i\cos\delta_o \\ \cos\delta_i\sin\delta_o \\ -\sin\delta_i \end{bmatrix}_{\mathcal{F}_B} \tag{6}$$

Next, we consider the total angular momentum $\boldsymbol{H}$. The total angular momentum of a spacecraft with a DGVSCMG can be described by

$$\boldsymbol{H} = \boldsymbol{J}\boldsymbol{\omega} + I_{go}\dot{\delta}_o\hat{\boldsymbol{g}}_o + I_{gi}\dot{\delta}_i\hat{\boldsymbol{g}}_i + I_{ws}\Omega\hat{\boldsymbol{s}}, \tag{7}$$

where $\boldsymbol{J} \in \mathbf{R}^{\mathbf{3}\times\mathbf{3}}$ is the inertia matrix of a spacecraft including a DGVSCMG, $\boldsymbol{\omega} \in \mathbf{R}^{\mathbf{3}}$ the angular velocity of the spacecraft, I_{gi} or I_{go} the moment of inertia of the DGVSCMG about the inner or

outer gimbal axis, respectively, I_{ws} the moment of inertia of the wheel about the DGVSCMG spin axis, and Ω the wheel spin rate. Assuming that no external torque is applied to the spacecraft body, the dynamics is given by

$$\dot{\boldsymbol{H}} + \boldsymbol{\omega}^{\times}\boldsymbol{H} = 0, \tag{8}$$

where the notation $\boldsymbol{x}^{\times}$ denotes the following skew-symmetric matrix:

$$\boldsymbol{x}^{\times} := \begin{bmatrix} 0 & -x_3 & x_2 \\ x_3 & 0 & -x_1 \\ -x_2 & x_1 & 0 \end{bmatrix}, \quad {}^{\forall}\boldsymbol{x} = [x_1\ x_2\ x_3]^T. \tag{9}$$

Substituting Eq. (7) into the first term of Eq. (8), we have

$$\boldsymbol{J}\dot{\boldsymbol{\omega}} + \left.\frac{d}{dt}\right|_{\mathcal{F}_B}(I_{go}\dot{\delta}_o\hat{\boldsymbol{g}}_o) + \left.\frac{d}{dt}\right|_{\mathcal{F}_B}(I_{gi}\dot{\delta}_i\hat{\boldsymbol{g}}_i) + \left.\frac{d}{dt}\right|_{\mathcal{F}_B}(I_{ws}\Omega\hat{\boldsymbol{s}}) + \boldsymbol{\omega}^{\times}\boldsymbol{H} = 0 \tag{10}$$

The second term of Eq. (10) is related to the outer gimbal of the DGVSCMG. Hence, we need not take account of the outer gimbal rotation. This is shown in the following way:

$$\left.\frac{d}{dt}\right|_{\mathcal{F}_B}(I_{go}\dot{\delta}_o\hat{\boldsymbol{g}}_o) = \left.\frac{d}{dt}\right|_{\mathcal{F}_{go}}(I_{go}\dot{\delta}_o\hat{\boldsymbol{g}}_o) + \dot{\delta}_o\hat{\boldsymbol{g}}_o{\times}I_{go}\dot{\delta}_o\hat{\boldsymbol{g}}_o = I_{go}\ddot{\delta}_o\hat{\boldsymbol{g}}_o \tag{11}$$

The third term of Eq. (10) is related to the inner gimbal of the DGVSCMG. In this case, when we consider the time derivative at the body-fixed frame, we must take account of the outer gimbal rotation. This is shown in the following way:

$$\begin{aligned}
\left.\frac{d}{dt}\right|_{\mathcal{F}_B}(I_{gi}\dot{\delta}_i\hat{\boldsymbol{g}}_i) &= \left.\frac{d}{dt}\right|_{\mathcal{F}_{go}}(I_{gi}\dot{\delta}_i\hat{\boldsymbol{g}}_i) + \dot{\delta}_o\hat{\boldsymbol{g}}_o{\times}I_{gi}\dot{\delta}_i\hat{\boldsymbol{g}}_i && (12)\\
&= \left.\frac{d}{dt}\right|_{\mathcal{F}_{gi}}(I_{gi}\dot{\delta}_i\hat{\boldsymbol{g}}_i) + \dot{\delta}_i\hat{\boldsymbol{g}}_i{\times}I_{gi}\dot{\delta}_i\hat{\boldsymbol{g}}_i + \dot{\delta}_o\hat{\boldsymbol{g}}_o{\times}I_{gi}\dot{\delta}_i\hat{\boldsymbol{g}}_i && (13)\\
&= I_{gi}\ddot{\delta}_i\hat{\boldsymbol{g}}_i + \dot{\delta}_o\hat{\boldsymbol{g}}_o{\times}I_{gi}\dot{\delta}_i\hat{\boldsymbol{g}}_i && (14)
\end{aligned}$$

The fourth term of Eq. (10) is related to the wheel spin rate of the DGVSCMG. Therefore, we must take account of both outer gimbal and inner gimbal rotations. This is shown in the following way:

$$\begin{aligned}
\left.\frac{d}{dt}\right|_{\mathcal{F}_B}(I_{ws}\Omega\hat{\boldsymbol{s}}) &= \left.\frac{d}{dt}\right|_{\mathcal{F}_{go}}(I_{ws}\Omega\hat{\boldsymbol{s}}) + \dot{\delta}_o\hat{\boldsymbol{g}}_{\boldsymbol{o}}{\times}I_{ws}\Omega\hat{\boldsymbol{s}} && (15)\\
&= \left.\frac{d}{dt}\right|_{\mathcal{F}_{gi}}(I_{ws}\Omega\hat{\boldsymbol{s}}) + \dot{\delta}_i\hat{\boldsymbol{g}}_{\boldsymbol{i}}{\times}I_{ws}\Omega\hat{\boldsymbol{s}} + \dot{\delta}_o\hat{\boldsymbol{g}}_{\boldsymbol{o}}{\times}I_{ws}\Omega\hat{\boldsymbol{s}} && (16)\\
&= \left.\frac{d}{dt}\right|_{\mathcal{F}_s}(I_{ws}\Omega\hat{\boldsymbol{s}}) + \dot{\delta}_i\hat{\boldsymbol{g}}_{\boldsymbol{i}}{\times}I_{ws}\Omega\hat{\boldsymbol{s}} + \dot{\delta}_o\hat{\boldsymbol{g}}_{\boldsymbol{o}}{\times}I_{ws}\Omega\hat{\boldsymbol{s}} && (17)\\
&= I_{ws}\dot{\Omega}\hat{\boldsymbol{s}} + I_{ws}\Omega\dot{\delta}_i\hat{\boldsymbol{g}}_{\boldsymbol{i}}{\times}\hat{\boldsymbol{s}} + I_{ws}\Omega\dot{\delta}_o\hat{\boldsymbol{g}}_{\boldsymbol{o}}{\times}\hat{\boldsymbol{s}} && (18)
\end{aligned}$$

Since $\ddot{\delta}_i$ and $\ddot{\delta}_o$ are small enough, compared with the other terms, $\ddot{\delta}_i$ and $\ddot{\delta}_o$ can be regarded as zero. In summary, Eq. (10) can be rewritten into

$$\boldsymbol{J}\dot{\boldsymbol{\omega}} + I_{gi}\dot{\delta}_i\dot{\delta}_o\hat{\boldsymbol{g}}_o{\times}\hat{\boldsymbol{g}}_i + I_{ws}\dot{\Omega}\hat{\boldsymbol{s}} + I_{ws}\Omega\dot{\delta}_i\hat{\boldsymbol{g}}_i{\times}\hat{\boldsymbol{s}} + I_{ws}\Omega\dot{\delta}_o\hat{\boldsymbol{g}}_o{\times}\hat{\boldsymbol{s}} + \boldsymbol{\omega}^{\times}\boldsymbol{H} = 0. \tag{19}$$

This is a generalized description of the spacecraft dynamics with a DGVSCMG. In this formula, by setting $\dot{\delta}_o = 0$ (corresponding to the case of the outer gimbal lock), one can get the dynamics of a SGVSCMG as follows:

$$\boldsymbol{J}\dot{\boldsymbol{\omega}} + I_{ws}\dot{\Omega}\hat{\boldsymbol{s}} + I_{ws}\Omega\dot{\delta}_i\hat{\boldsymbol{g}}_i{\times}\hat{\boldsymbol{s}} + \boldsymbol{\omega}^{\times}\boldsymbol{H} = 0 \tag{20}$$

In Eq. (19), by setting $\dot{\Omega} = 0$, one can get the dynamics of a DGCMG as follows:

$$\boldsymbol{J}\dot{\boldsymbol{\omega}} + I_{gi}\dot{\delta}_i\dot{\delta}_o\hat{\boldsymbol{g}}_o{\times}\hat{\boldsymbol{g}}_i + I_{ws}\Omega\dot{\delta}_i\hat{\boldsymbol{g}}_i{\times}\hat{\boldsymbol{s}} + I_{ws}\Omega\dot{\delta}_o\hat{\boldsymbol{g}}_o{\times}\hat{\boldsymbol{s}} + \boldsymbol{\omega}^{\times}\boldsymbol{H} = 0 \tag{21}$$

In Eq. (19), by setting $\dot{\delta}_o = 0$ and $\dot{\Omega} = 0$, one can get the dynamics of a SGCMG as follows:

$$\boldsymbol{J}\dot{\boldsymbol{\omega}} + I_{ws}\Omega\dot{\delta}_i\hat{\boldsymbol{g}}_i{\times}\hat{\boldsymbol{s}} + \boldsymbol{\omega}^{\times}\boldsymbol{H} = 0 \tag{22}$$

In Eq. (19), by setting $\dot{\delta}_o = 0$ and $\dot{\delta}_i = 0$, one can get the dynamics of a RW as follows:

$$\boldsymbol{J}\dot{\boldsymbol{\omega}} + I_{ws}\dot{\Omega}\hat{\boldsymbol{s}} + \boldsymbol{\omega}^{\times}\boldsymbol{H} = 0 \tag{23}$$

Therefore, the spacecraft dynamics with a DGVSCMG in Eq. (19) itself can express all MEDs.

Kinematics

The quaternion consists of the vector part and the scalar one. Given the principal rotation axis $\hat{\boldsymbol{\alpha}} = [\alpha_x\ \alpha_y\ \alpha_z]^T$ with $\hat{\boldsymbol{\alpha}}^T\hat{\boldsymbol{\alpha}} = 1$ and the rotation angle Θ, the quaternion (Euler Parameter) is defined by

$$\boldsymbol{q} = \begin{bmatrix}\bar{\boldsymbol{q}}\\ q_4\end{bmatrix} := \begin{bmatrix}\hat{\boldsymbol{\alpha}}\sin\frac{\Theta}{2}\\ \cos\frac{\Theta}{2}\end{bmatrix}, \tag{24}$$

with the constraint:

$$\boldsymbol{q}^T\boldsymbol{q} = \hat{\boldsymbol{\alpha}}^T\hat{\boldsymbol{\alpha}}\sin^2\frac{\Theta}{2} + \cos^2\frac{\Theta}{2} = 1. \tag{25}$$

To formulate the attitude tracking problem of a spacecraft, we need the error quaternion $\boldsymbol{q}_e = \boldsymbol{q}^{\dagger}\boldsymbol{q}_d$, where $\boldsymbol{q}$ denotes the current quaternion and $\boldsymbol{q}_d$ denotes the desired quaternion. The kinematics equation is given by

$$\begin{bmatrix}\dot{\bar{\boldsymbol{q}}}_e\\ \dot{q}_{4e}\end{bmatrix} = \boldsymbol{G}(\boldsymbol{q}_e)\boldsymbol{\omega}, \quad \boldsymbol{G}(\boldsymbol{q}_e) := \frac{1}{2}\begin{bmatrix}q_{4_e}\boldsymbol{I}_3 + \bar{\boldsymbol{q}}_e^{\times}\\ -\bar{\boldsymbol{q}}_e^T\end{bmatrix}. \tag{26}$$

GENERALIZED LPV MODEL AND CONTROLLER SYNTHESIS

The purpose of this research is to deal with complete attitude control via LPV control theory. First, let us transform Eq. (19) into an LPV model. The Jacobian linearization of Eq. (19) around the equilibrium point ($\boldsymbol{\omega}_{eq} = 0$, $\dot{\Omega}_{eq} = 0$, $\dot{\delta}_{i_{eq}} = 0$, $\dot{\delta}_{o_{eq}} = 0$) leads to the linear dynamics of a spacecraft with a DGVSCMG. The spacecraft dynamics and the kinematics equations based on the quaternion are given as follows:

$$\begin{cases} \dot{\boldsymbol{\omega}} = \boldsymbol{A}(\boldsymbol{\rho})\boldsymbol{\omega} + \boldsymbol{B}(\boldsymbol{\rho})\boldsymbol{u} \\ \dot{\bar{\boldsymbol{q}}}_e = \bar{\boldsymbol{G}}(\bar{\boldsymbol{q}}_e)\boldsymbol{\omega} \end{cases}, \quad \bar{\boldsymbol{G}}(\bar{\boldsymbol{q}}_e) = \frac{1}{2}(q_{4_e}\boldsymbol{I}_3 + \bar{\boldsymbol{q}}_e^{\times}), \tag{27}$$

where $\boldsymbol{u} = [\dot{\Omega}\ \dot{\delta}_i\ \dot{\delta}_o]^T$,

$$\begin{aligned} \boldsymbol{A}(\boldsymbol{\rho}) &= I_{ws}\Omega\boldsymbol{J}^{-1}[\hat{\boldsymbol{s}}]^{\times} && (28) \\ &= I_{ws}\boldsymbol{J}^{-1}\begin{bmatrix} 0 & \Omega\sin\delta_i & \Omega\cos\delta_i\sin\delta_o \\ -\Omega\sin\delta_i & 0 & -\Omega\cos\delta_i\cos\delta_o \\ -\Omega\cos\delta_i\sin\delta_o & \Omega\cos\delta_i\cos\delta_o & 0 \end{bmatrix}, && (29) \end{aligned}$$

and

$$\begin{aligned} \boldsymbol{B}(\boldsymbol{\rho}) &= -I_{ws}\boldsymbol{J}^{-1}[\hat{\boldsymbol{s}}\ \ \Omega\hat{\boldsymbol{g}}_i\times\hat{\boldsymbol{s}}\ \ \Omega\hat{\boldsymbol{g}}_o\times\hat{\boldsymbol{s}}] && (30) \\ &= I_{ws}\boldsymbol{J}^{-1}\begin{bmatrix} -\cos\delta_i\cos\delta_o & \Omega\sin\delta_i\cos\delta_o & \Omega\cos\delta_i\sin\delta_o \\ -\cos\delta_i\sin\delta_o & \Omega\sin\delta_i\sin\delta_o & -\Omega\cos\delta_i\cos\delta_o \\ \sin\delta_i & \Omega\cos\delta_i & 0 \end{bmatrix}, && (31) \end{aligned}$$

where $\boldsymbol{\rho} = [\Omega\ \ \delta_i\ \ \delta_o]^T$ and $\bar{\boldsymbol{q}}_e = [q_1\ q_2\ q_3]^T$ are the scheduling parameter vectors. Note that only the vector part of the quaternion $\boldsymbol{q}$ is included in Eq. (27), since the scalar one can be determined by the vector one from the constraint of Eq. (25). If $\boldsymbol{\rho}$ is rewritten by $\boldsymbol{\rho} = [\Omega\ \ \sin\delta_i\ \ \cos\delta_i\ \ \sin\delta_o\ \ \cos\delta_o]^T$ with $\bar{\boldsymbol{q}}_e = [q_1\ q_2\ q_3]^T$, this system is covered with a convex hull which has $256(= 2^8)$ extreme points or vertices.[17] However, the scheduling parameter of this LPV model in Eq. (27) has too many vertices to perform the GS controller design. To overcome this problem, we shall develop several methods to reduce the number of vertices. First, we embed the part which depends on the scheduling parameter of the coefficient matrix $\boldsymbol{B}(\boldsymbol{\rho})$ into a new input $\boldsymbol{u}'$ as follows:

$$\begin{cases} \boldsymbol{B} := I_{ws}\boldsymbol{J}^{-1} \\ \boldsymbol{u}' := \begin{bmatrix} -\cos\delta_i\cos\delta_o & \Omega\sin\delta_i\cos\delta_o & \Omega\cos\delta_i\sin\delta_o \\ -\cos\delta_i\sin\delta_o & \Omega\sin\delta_i\sin\delta_o & -\Omega\cos\delta_i\cos\delta_o \\ \sin\delta_i & \Omega\cos\delta_i & 0 \end{bmatrix}\begin{bmatrix} \dot{\Omega} \\ \dot{\delta}_i \\ \dot{\delta}_o \end{bmatrix} \end{cases} \tag{32}$$

Therefore, setting the state variable $\boldsymbol{x} := [\boldsymbol{\omega}^T\ \bar{\boldsymbol{q}}_e^T]^T$, the state-space representation of Eq. (27) can be rewritten as follows:

$$\begin{aligned} \begin{bmatrix} \dot{\boldsymbol{\omega}} \\ \dot{\bar{\boldsymbol{q}}}_e \end{bmatrix} &= \begin{bmatrix} \boldsymbol{A}(\boldsymbol{\rho}) & 0 \\ \bar{\boldsymbol{G}}(\bar{\boldsymbol{q}}_e) & 0 \end{bmatrix}\begin{bmatrix} \boldsymbol{\omega} \\ \bar{\boldsymbol{q}}_e \end{bmatrix} + \begin{bmatrix} \boldsymbol{B} \\ 0 \end{bmatrix}\boldsymbol{u}' && (33) \\ &\Leftrightarrow \dot{\boldsymbol{x}} = \boldsymbol{A}_e(\boldsymbol{\rho},\, \bar{\boldsymbol{q}}_e)\boldsymbol{x} + \boldsymbol{B}_e\boldsymbol{u}', && (34) \end{aligned}$$

where

$$\boldsymbol{A}_e(\boldsymbol{\rho},\, \bar{\boldsymbol{q}}_e) := \begin{bmatrix} \boldsymbol{A}(\boldsymbol{\rho}) & 0 \\ \bar{\boldsymbol{G}}(\bar{\boldsymbol{q}}_e) & 0 \end{bmatrix}, \quad \boldsymbol{B}_e := \begin{bmatrix} \boldsymbol{B} \\ 0 \end{bmatrix}. \tag{35}$$

Although the vector part of the error quaternion also should be regarded as a scheduling parameter related to kinematics, next, we shall eliminate this parameter from the coefficient matrix to reduce the number of scheduling parameters. By using PDCT (Parameter-Dependent Coordinate Transformation) matrix:

$$\boldsymbol{T} := \begin{bmatrix} \boldsymbol{I}_3 & 0 \\ 0 & \bar{\boldsymbol{G}}(\bar{\boldsymbol{q}}_e)^{-1} \end{bmatrix}, \tag{36}$$

while introducing a virtual state $\boldsymbol{\zeta}$ with $\dot{\boldsymbol{\zeta}} := \boldsymbol{G}(\bar{\boldsymbol{q}}_e)^{-1}\dot{\bar{\boldsymbol{q}}}_e$, we obtain the following simple LPV model which is easy to use for control design. By using $\boldsymbol{T}$, Eq. (33) can be expressed as follows:

$$\boldsymbol{T}\begin{bmatrix} \dot{\boldsymbol{\omega}} \\ \dot{\bar{\boldsymbol{q}}}_e \end{bmatrix} = \boldsymbol{T}\begin{bmatrix} \boldsymbol{A}(\boldsymbol{\rho}) & 0 \\ \bar{\boldsymbol{G}}(\bar{\boldsymbol{q}}_e) & 0 \end{bmatrix}\boldsymbol{T}^{-1}\boldsymbol{T}\begin{bmatrix} \boldsymbol{\omega} \\ \bar{\boldsymbol{q}}_e \end{bmatrix} + \boldsymbol{T}\begin{bmatrix} \boldsymbol{B} \\ 0 \end{bmatrix}\boldsymbol{u}' \tag{37}$$

$$\begin{bmatrix} \dot{\boldsymbol{\omega}} \\ \bar{\boldsymbol{G}}(\bar{\boldsymbol{q}}_e)^{-1}\dot{\bar{\boldsymbol{q}}}_e \end{bmatrix} = \begin{bmatrix} \boldsymbol{A}(\boldsymbol{\rho}) & 0 \\ \boldsymbol{I}_3 & 0 \end{bmatrix}\begin{bmatrix} \boldsymbol{\omega} \\ \bar{\boldsymbol{G}}(\bar{\boldsymbol{q}}_e)^{-1}\bar{\boldsymbol{q}}_e \end{bmatrix} + \begin{bmatrix} \boldsymbol{B} \\ 0 \end{bmatrix}\boldsymbol{u}' \tag{38}$$

$$\begin{bmatrix} \dot{\boldsymbol{\omega}} \\ \dot{\boldsymbol{\zeta}} \end{bmatrix} = \begin{bmatrix} \boldsymbol{A}(\boldsymbol{\rho}) & 0 \\ \boldsymbol{I}_3 & 0 \end{bmatrix}\begin{bmatrix} \boldsymbol{\omega} \\ \boldsymbol{\zeta} \end{bmatrix} + \begin{bmatrix} \boldsymbol{B} \\ 0 \end{bmatrix}\boldsymbol{u} \tag{39}$$

$$\Leftrightarrow \dot{\tilde{\boldsymbol{x}}} = \tilde{\boldsymbol{A}}_e(\boldsymbol{\rho})\tilde{\boldsymbol{x}} + \tilde{\boldsymbol{B}}_e\boldsymbol{u}', \tag{40}$$

where $\tilde{\boldsymbol{x}} := [\boldsymbol{\omega}^T\ \boldsymbol{\zeta}^T]^T$ and

$$\tilde{\boldsymbol{A}}_e(\boldsymbol{\rho}) := \begin{bmatrix} \boldsymbol{A}(\boldsymbol{\rho}) & 0 \\ \boldsymbol{I}_3 & 0 \end{bmatrix}, \quad \tilde{\boldsymbol{B}}_e := \begin{bmatrix} \boldsymbol{B} \\ 0 \end{bmatrix}. \tag{41}$$

Note that $\boldsymbol{\zeta} \neq \bar{\boldsymbol{G}}(\bar{\boldsymbol{q}}_e)^{-1}\bar{\boldsymbol{q}}_e$ in Eq. (38) has been replaced by $\boldsymbol{\zeta}$ in Eq. (39), since this part is eliminated by the premultiplied matrix. The GS controller designed to this simple LPV model guarantees overall stability and control performance for the original plant as in Eq. (34). This controller is given by

$$\boldsymbol{u} = -\tilde{\boldsymbol{K}}(\boldsymbol{\rho})\tilde{\boldsymbol{x}}. \tag{42}$$

Figure 2 shows the relationship of two plants in Eq. (34) and Eq. (40). The scheduling parameter $\boldsymbol{\rho}$ of this simple LPV model is given by

$$\boldsymbol{\rho} = [\Omega \sin\delta_i,\ \Omega\cos\delta_i \sin\delta_o,\ \Omega\cos\delta_i\cos\delta_o]^T, \tag{43}$$

After these operations, the number of vertices has been reduced into $8(=2^3)$. Setting $p = 8$ as the

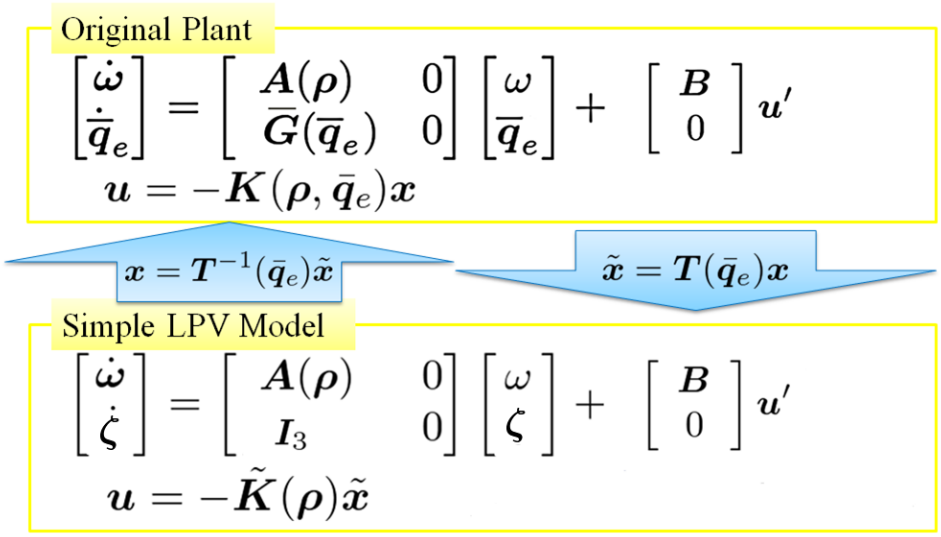

Figure 2. Relationship of two plants.

number of the vertices, the LPV system can be expressed by the following polytopic representation:

$$\boldsymbol{A}(\boldsymbol{\rho}) \quad = \sum_{i=1}^{p} \lambda_i(\boldsymbol{\rho}) \boldsymbol{A}_i \tag{44}$$

where

$$\sum_{i=1}^{p} \lambda_i(\boldsymbol{\rho}) = 1, \quad \lambda_i(\boldsymbol{\rho}) \geq 0. \tag{45}$$

Now, we consider a GS controller $\tilde{\boldsymbol{K}}(\boldsymbol{\rho})$ that guarantees overall stability and achieves $\mathcal{H}_2$ performance for the simple LPV model as in Eq. (40). First, we introduce the generalized plant for Eq. (34) and that for Eq. (40) defined as follows:

$$\begin{cases} \dot{\boldsymbol{x}} = A_e(\boldsymbol{\rho}, \bar{\boldsymbol{q}}_e)\boldsymbol{x} + B_e\boldsymbol{u}' + E\boldsymbol{w} \\ \boldsymbol{z} = C\boldsymbol{x} + D\boldsymbol{u}' \end{cases} \quad \text{(Generalized plant for the original plant)} \tag{46}$$

$$\begin{cases} \dot{\tilde{\boldsymbol{x}}} = \tilde{A}_e(\boldsymbol{\rho})\tilde{\boldsymbol{x}} + \tilde{B}_e\boldsymbol{u}' + \tilde{E}\boldsymbol{w} \\ \tilde{\boldsymbol{z}} = \tilde{C}\tilde{\boldsymbol{x}} + \tilde{D}\boldsymbol{u}' \end{cases} \quad \text{(Generalized plant for the simple LPV model)} \tag{47}$$

where the coefficient matrix sets (C, D) and $(\tilde{C}, \tilde{D})$ are selected such that they normally satisfy the condition $C'D = 0, D'D > 0$, $\tilde{C}'\tilde{D} = 0$, and $\tilde{D}'\tilde{D} > 0$, and where $\boldsymbol{w}, \boldsymbol{z}$, and $\tilde{\boldsymbol{z}}$ are the disturbance input vector, the performance output vector for the original plant as in Eq. (34), and that for the simple LPV model as in Eq. (40), respectively. Then, we consider the following LMI problem:

$$\begin{aligned} &\inf_{\boldsymbol{W}_i, \boldsymbol{X}_i, \boldsymbol{Z}_i} [\text{Trace } (\boldsymbol{Z}_i)] \quad \text{subject to} \\ &\Phi_0(\boldsymbol{X}_i, \boldsymbol{Z}_i) > 0, \ \Psi_{\mathcal{H}_2}(\boldsymbol{W}_i, \boldsymbol{X}_i) < 0, \quad 1 \leq i \leq p \end{aligned} \tag{48}$$

where

$$\Psi_{\mathcal{H}_2}(\boldsymbol{W}_i,\, \boldsymbol{X}_i) := \begin{bmatrix} (\boldsymbol{A}_i\boldsymbol{X}_i - \boldsymbol{B}\boldsymbol{W}_i) + (\ \bullet\ )^T & * \\ \boldsymbol{C}\boldsymbol{X}_i - \boldsymbol{D}\boldsymbol{W}_i & -\boldsymbol{I} \end{bmatrix},\ \Phi_0(\boldsymbol{X}_i,\, \boldsymbol{Z}_i) := \begin{bmatrix} \boldsymbol{X}_i & * \\ \boldsymbol{E}^T & \boldsymbol{Z}_i \end{bmatrix}. \tag{49}$$

Using the optimal solution sets $\boldsymbol{X}_i, \boldsymbol{W}_i$ to the problem in Eq. (48), we have the extreme controllers:

$$\boldsymbol{K}_i = \boldsymbol{W}_i\boldsymbol{X}_i^{-1}, \quad 1 \le i \le p. \tag{50}$$

Then, the GS controller to the simple LPV model in Eq. (47) is constructed by

$$\tilde{\boldsymbol{K}}(\boldsymbol{\rho}) = \left\{ \sum_{i=1}^{p} \lambda_i \boldsymbol{K}_i : \lambda_i \ge 0,\ \sum_{i=1}^{p} \lambda_i = 1 \right\}. \tag{51}$$

Getting back the coordinate transformation $\boldsymbol{x} := \boldsymbol{T}^{-1}(\bar{\boldsymbol{q}}_e)\tilde{\boldsymbol{x}}$, this GS controller can be transformed into the controller $\boldsymbol{K}(\boldsymbol{\rho}, \bar{\boldsymbol{q}}_e)$ corresponding to the original plant in Eq. (46) as follows:

$$\boldsymbol{u} = -\tilde{\boldsymbol{K}}(\boldsymbol{\rho})\tilde{\boldsymbol{x}} = -\tilde{\boldsymbol{K}}(\boldsymbol{\rho})\boldsymbol{T}(\bar{\boldsymbol{q}}_e)\boldsymbol{T}(\bar{\boldsymbol{q}}_e)^{-1}\tilde{\boldsymbol{x}} = -\boldsymbol{K}(\boldsymbol{\rho}, \bar{\boldsymbol{q}}_e)\boldsymbol{x}, \tag{52}$$

where

$$\boldsymbol{K}(\boldsymbol{\rho},\, \bar{\boldsymbol{q}}_e) := \tilde{\boldsymbol{K}}(\boldsymbol{\rho})\boldsymbol{T}(\bar{\boldsymbol{q}}_e). \tag{53}$$

The design procedure described above is summarized in Figure 2.

SINGULARITY ANALYSIS

From Eq. (32), the steering law is described as follows:

$$\boldsymbol{u}' = \boldsymbol{F}\begin{bmatrix} \dot{\Omega} \\ \dot{\delta}_i \\ \dot{\delta}_o \end{bmatrix}, \quad \boldsymbol{F} := \begin{bmatrix} -\cos\delta_i\cos\delta_o & \Omega\sin\delta_i\cos\delta_o & \Omega\cos\delta_i\sin\delta_o \\ -\cos\delta_i\sin\delta_o & \Omega\sin\delta_i\sin\delta_o & -\Omega\cos\delta_i\cos\delta_o \\ \sin\delta_i & \Omega\cos\delta_i & 0 \end{bmatrix} \tag{54}$$

If $\text{rank}(\boldsymbol{F}) = 3$, we can always solve Eq. (54) for any given torque command $\boldsymbol{u}'$. In $\text{rank}(\boldsymbol{F}) \neq 3$, we cannot solve it. It occurs when $\det(\boldsymbol{F}) = 0$ with

$$\det(\boldsymbol{F}) = \det\begin{bmatrix} -\cos\delta_i\cos\delta_o & \Omega\sin\delta_i\cos\delta_o & \Omega\cos\delta_i\sin\delta_o \\ -\cos\delta_i\sin\delta_o & \Omega\sin\delta_i\sin\delta_o & -\Omega\cos\delta_i\cos\delta_o \\ \sin\delta_i & \Omega\cos\delta_i & 0 \end{bmatrix} = -\Omega^2\cos\delta_i. \tag{55}$$

When $\Omega = 0$ or $\cos\delta_i = 0$, the DGVSCMG system falls into a singularity. Accordingly, we need to use the controller under the condition of $\Omega \neq 0$, $-90[\text{deg}] < \delta_i < 90[\text{deg}]$.

Table 1. Simulation parameters, initial condition, and desired quaternion.

Symbol	Value	Unit
J	diag[10 10 8]	kgm^2
I_{ws}	0.0042	kgm^2
I_{gi}	0.001	kgm^2
I_{go}	0.001	kgm^2
$\boldsymbol{q}_0$	$[0\ 0\ 0\ 1]^T$	–
$\boldsymbol{\omega}_0$	$[0.03\ -0.02\ 0.04]^T$	rad/s
Ω_0	300	rad/s
Ω_{max}	700	rad/s
δ_{i0}	0	deg
δ_{o0}	0	deg
$\boldsymbol{q}_d$	$[-0.2\ 0.2\ 0.75\ 0.6]^T$	–

NUMERICAL SIMULATION

This section presents some numerical simulations of the proposed method and two conventional (Hamilton-Jacobi equation-based and Lyapunov function-based) methods. The simulation parameters, the initial condition, and the desired quaternion are given in Table 1. The controller design parameters $\boldsymbol{C}$ and $\boldsymbol{D}$ are given by

$$\boldsymbol{C} = \begin{bmatrix} 3 \times \boldsymbol{I}_3 & 0_{3\times3} \\ 0_{3\times3} & \boldsymbol{I}_3 \\ 0_{3\times3} & 0_{3\times3} \end{bmatrix}, \quad \boldsymbol{D} = \begin{bmatrix} 0_{6\times3} \\ 0.03 \times \boldsymbol{I}_3 \end{bmatrix}. \tag{56}$$

Figures 3-8 and 9-14 show the simulation results by using the Lyapunov function-based controller and the Hamilton-Jacobi equation-based controller, respectively. On the other hand, Figures 15-20 show the simulation result by using the proposed GS controller. From these figures, compared with the conventional controllers, the proposed controller has achieved better performance.

With the Lyapunov function-based controller as in Figures 3-8, overall stability of attitude control is always guaranteed. However, control performance is ignored in most cases. With the Hamilton-Jacobi equation-based controller as in Figures 9-14, overall stability and control performance is always guaranteed. However, control performance is to be attained not in absolute optimality but in asymptotic optimality. In contrast, the proposed method as in Figures 15-20 guarantees both overall stability and control performance. And compared with the conventional methods, it has considerably improved control performance. Comparison of three types of controllers are summarized in Table 2.

Table 2. Comparison of three types controllers.

Technique	Lyapunov Control Theory	H.J.-Based Control Theory	LPV Control Theory
Stability	Guaranteed	Guaranteed	Guaranteed
Control Performance	Almost Impossible	Possible	Guaranteed
Controller Type	Fixed	Fixed	Gain-Scheduled

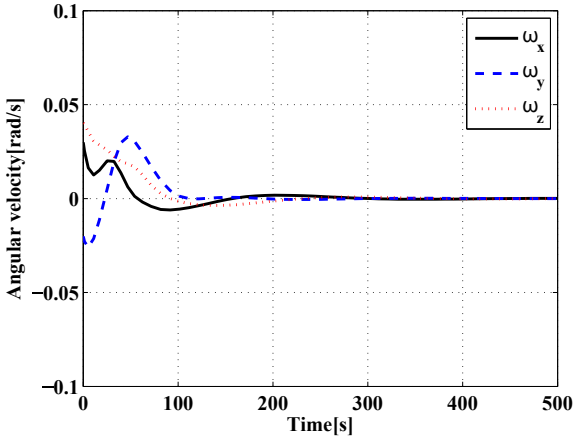

Figure 3. Angular velocity (Lyapunov-based).

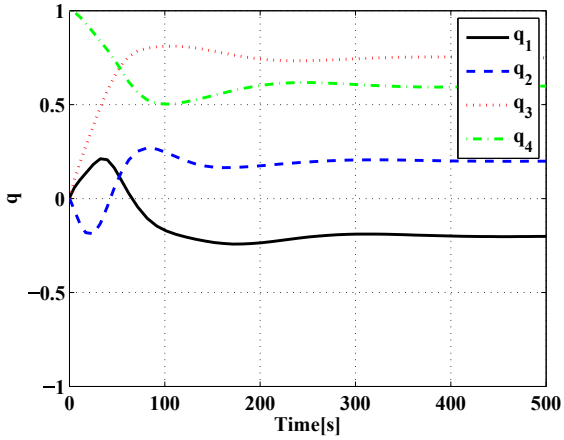

Figure 4. Quaternion (Lyapunov-based).

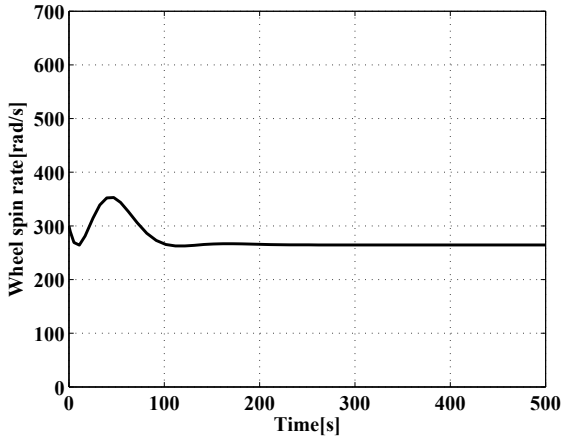

Figure 5. Wheel spin rate (Lyapunov-based).

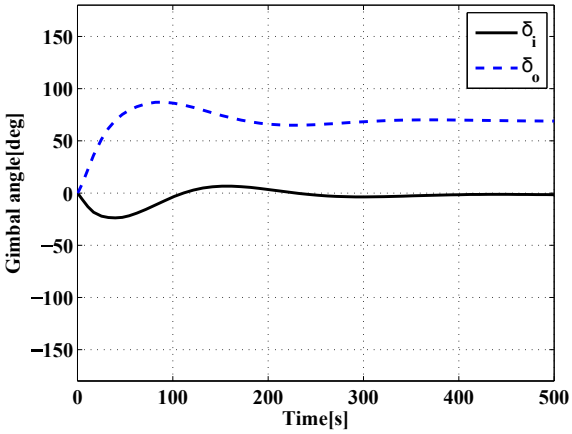

Figure 6. Gimbal angle (Lyapunov-based).

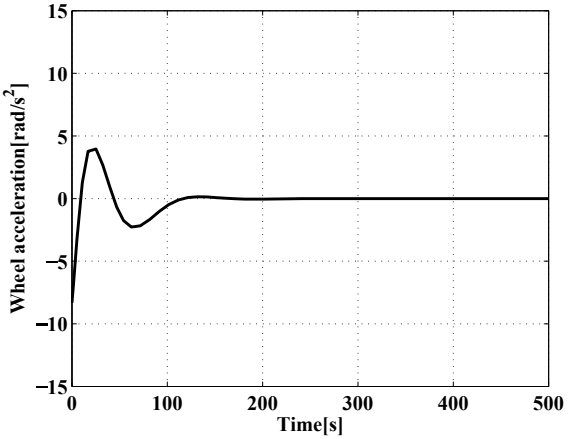

Figure 7. Wheel acceleration (Lyapunov-based).

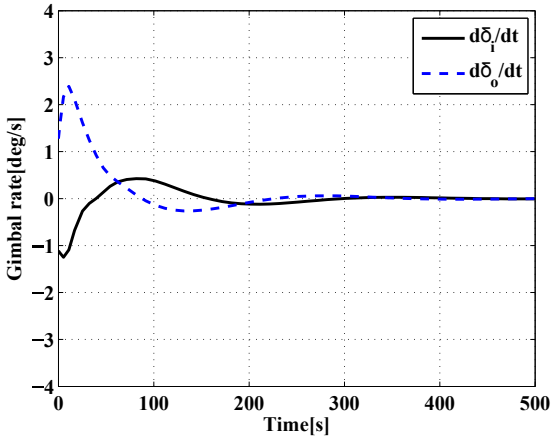

Figure 8. Gimbal rate (Lyapunov-based).

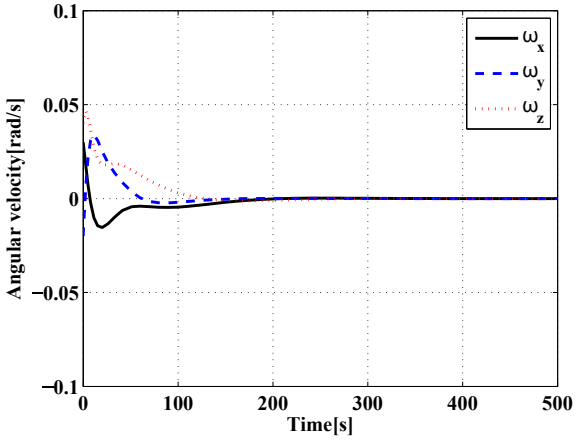

Figure 9. Angular velocity (H.J.-based).

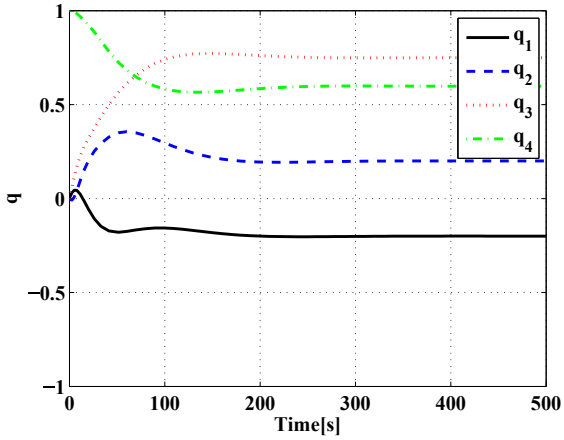

Figure 10. Quaternion (H.J.-based).

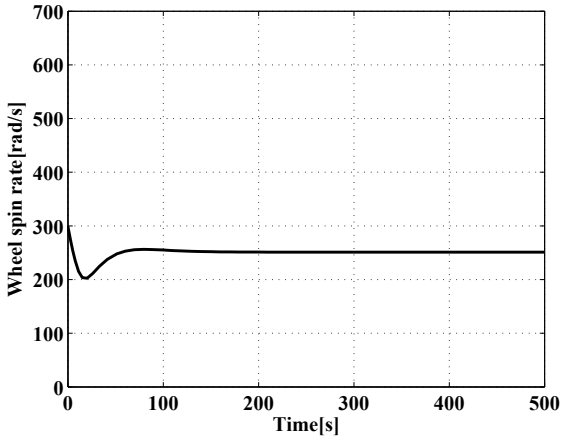

Figure 11. Wheel spin rate (H.J.-based).

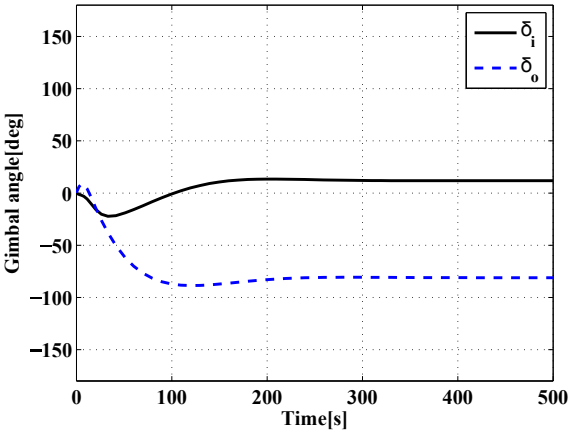

Figure 12. Gimbal angle (H.J.-based).

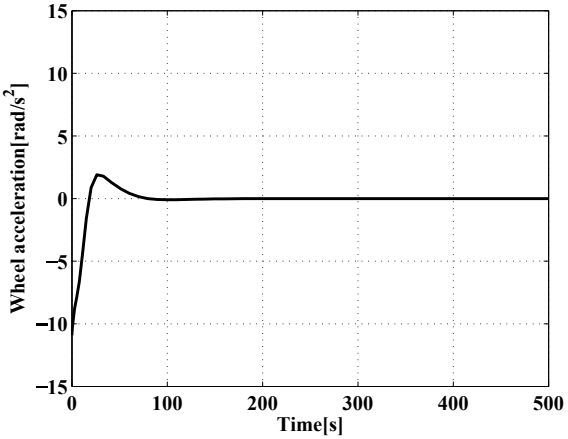

Figure 13. Wheel acceleration (H.J.-based).

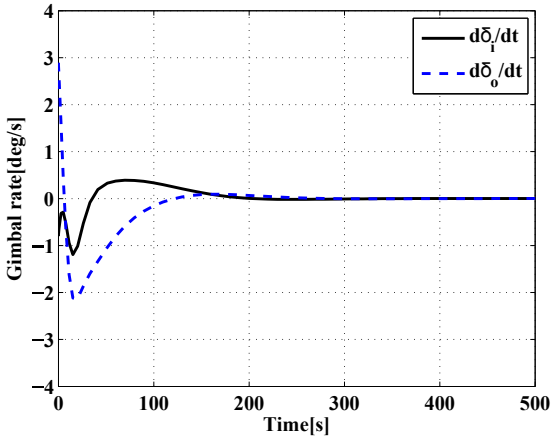

Figure 14. Gimbal rate (H.J.-based).

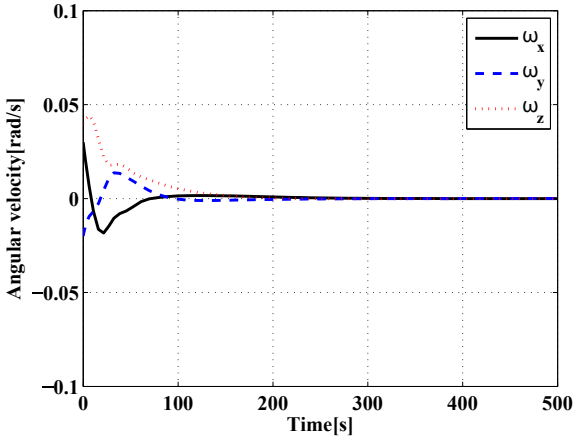

Figure 15. Angular velocity (LPV theory).

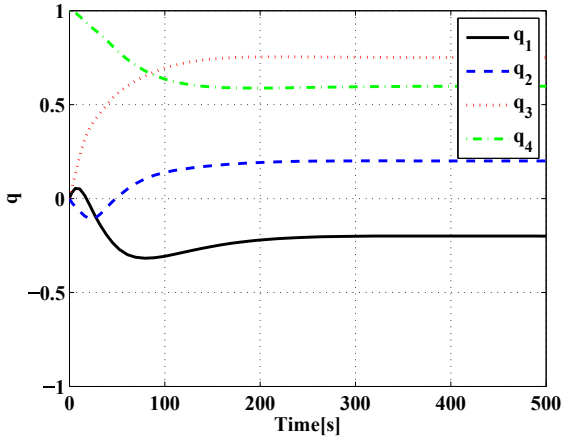

Figure 16. Quaternion (LPV theory).

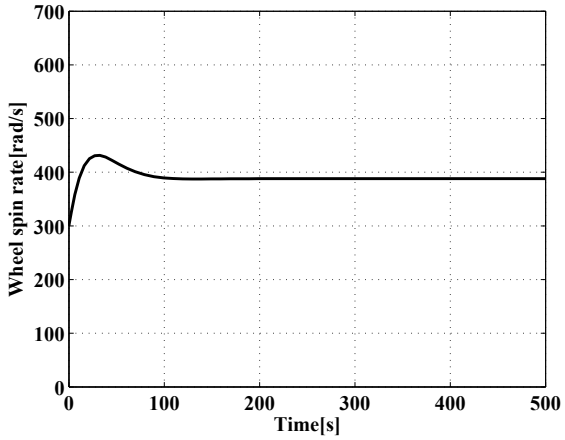

Figure 17. Wheel spin rate (LPV theory).

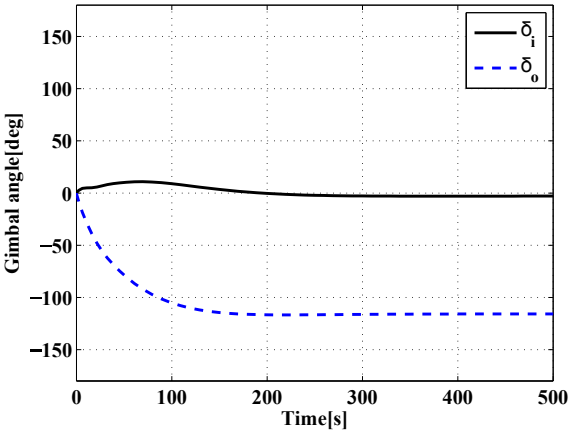

Figure 18. Gimbal angle (LPV theory).

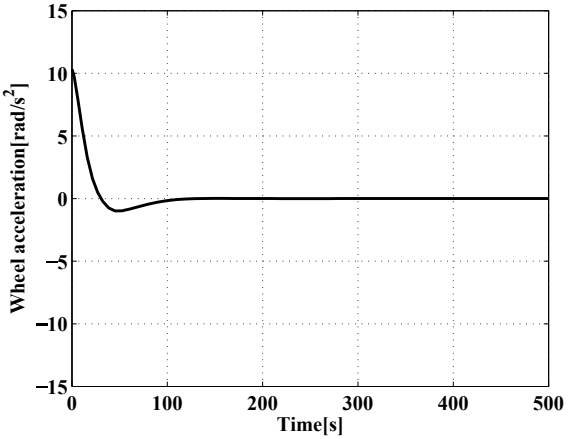

Figure 19. Wheel acceleration (LPV theory).

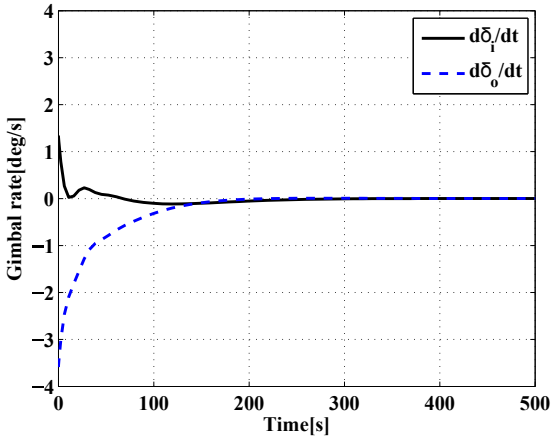

Figure 20. Gimbal rate (LPV theory).

CONCLUSION

In this paper, we considered dynamics and kinematics of a spacecraft with a DGVSCMG. And we have proposed a new method for complete attitude control via LPV control theory, while newly introducing an interesting Parameter-Dependent Coordinate Transformation (PDCT) as well as a virtual state variable. Through a numerical example, we demonstrated the efficiency of the proposed method to compare with two conventional methods (Lyapunov function-based and Hamilton-Jacobi equation-based methods). As a result, the proposed method has considerably improved control performance.

ACKNOWLEDGMENT

The authors acknowledge helpful advices from N. Sakuramata and Y. Yamamoto.

APPENDIX A: CONVENTIONAL METHODS

Hamilton-Jacobi equation-based controller

First, we consider the following evaluation function:

$$\mathcal{J} = \frac{1}{2}\int_0^\infty \{k^2\|\bar{\boldsymbol{q}}_{\boldsymbol{e}}(t)\|^2 + \|\boldsymbol{\omega}(t)\|^2\}dt. \tag{57}$$

For this function, we have the Hamilton-Jacobi equation:

$$\frac{\partial W}{\partial \boldsymbol{q_e}}[G(\boldsymbol{q_e})\boldsymbol{\omega}] + \frac{1}{2}k^2\|\bar{\boldsymbol{q}}_{\boldsymbol{e}}\|^2 + \frac{1}{2}\|\boldsymbol{\omega}(t)\|^2 = 0. \tag{58}$$

Next, we minimize the evaluation function $\mathcal{J}$ by using completing the square.

$$\frac{1}{2}\left\|\boldsymbol{\omega} + G(\boldsymbol{q_e})^T\frac{\partial^T W}{\partial \boldsymbol{q_e}}\right\|^2 + \frac{k^2}{2}\|\bar{\boldsymbol{q}}_{\boldsymbol{e}}\|^2 - \frac{1}{2}\left\|G(\boldsymbol{q_e})^T\frac{\partial^T W}{\partial \boldsymbol{q_e}}\right\|^2 = 0 \tag{59}$$

Therefore, we determine the generating function W in order that $\mathcal{J}$ may be the minimum. For example, defining $W = 2k(-q_{4e} + C)$, $\boldsymbol{\omega}$ is given by

$$\boldsymbol{\omega} = -k\bar{\boldsymbol{q}}_{\boldsymbol{e}}. \tag{60}$$

Eq. (60) is the optimal control law derived from the Hamilton-Jacobi equation. Next, we consider the feedback control law:

$$\boldsymbol{u} = \boldsymbol{\omega}^\times \boldsymbol{H} - k\boldsymbol{J}\dot{\bar{\boldsymbol{q}}}_{\boldsymbol{e}} - \lambda\boldsymbol{J}(\boldsymbol{\omega} + k\bar{\boldsymbol{q}}_{\boldsymbol{e}}) \tag{61}$$

which is asymptotically equivalent to the optimal control law derived from the Hamilton-Jacobi equation. Dynamics of a DGVSCMG is given by

$$\boldsymbol{J}\dot{\boldsymbol{\omega}} = -\boldsymbol{\omega}^{\times}\boldsymbol{H} + \boldsymbol{u}. \tag{62}$$

$$\boldsymbol{u} = -I_{gi}\dot{\delta}_i\dot{\delta}_o\hat{\boldsymbol{g}}_o{\times}\hat{\boldsymbol{g}}_i - I_{ws}\dot{\Omega}\hat{\boldsymbol{s}} - I_{ws}\Omega\dot{\delta}_i\hat{\boldsymbol{g}}_i{\times}\hat{\boldsymbol{s}} - I_{ws}\Omega\dot{\delta}_o\hat{\boldsymbol{g}}_o{\times}\hat{\boldsymbol{s}} \tag{63}$$

Substituting Eq. (61) into Eq. (62), we have

$$\begin{aligned}\boldsymbol{J}\dot{\boldsymbol{\omega}} &= -\boldsymbol{\omega}^{\times}\boldsymbol{H} + \left\{\boldsymbol{\omega}^{\times}\boldsymbol{H} - k\boldsymbol{J}\dot{\bar{\boldsymbol{q}}}_{\boldsymbol{e}} - \lambda\boldsymbol{J}(\boldsymbol{\omega} + k\bar{\boldsymbol{q}}_{\boldsymbol{e}})\right\} &(64)\\ &\Longleftrightarrow (\dot{\boldsymbol{\omega}} + k\dot{\bar{\boldsymbol{q}}}_{\boldsymbol{e}}) = -\lambda(\boldsymbol{\omega} + k\bar{\boldsymbol{q}}_{\boldsymbol{e}}) &(65)\end{aligned}$$

Therefore, as $\lambda \to \infty$, we obtain the optimal control law $\boldsymbol{\omega}^* = -k\bar{\boldsymbol{q}}_{\boldsymbol{e}}$, asymptotically.

Lyapunov function-based controller

Lyapunov function to realize 3-axes attitude control is given by

$$V = \frac{1}{2}\boldsymbol{\omega}^T\boldsymbol{J}\boldsymbol{\omega} + k\left[(q_{4e}-1)^2 + \bar{\boldsymbol{q}}_{\boldsymbol{e}}^T\bar{\boldsymbol{q}}_{\boldsymbol{e}}\right], \quad k > 0. \tag{66}$$

Differentiating Eq. (66) with respect to time, we have

$$\dot{V} = \boldsymbol{\omega}^T\boldsymbol{J}\dot{\boldsymbol{\omega}} + k\left[2(q_{4e}-1)\dot{q_{4e}} + 2\bar{\boldsymbol{q}}_{\boldsymbol{e}}^T\dot{\bar{\boldsymbol{q}}}_{\boldsymbol{e}}\right]. \tag{67}$$

Substituting Eq. (26) and Eq. (62) into Eq. (67), we have

$$\begin{aligned}\dot{V} &= -\boldsymbol{\omega}^T\boldsymbol{u} + k\left[-(q_{4e}-1)\bar{\boldsymbol{q}}_{\boldsymbol{e}}^T + \bar{\boldsymbol{q}}_{\boldsymbol{e}}^T(q_{4e}\boldsymbol{I}_3 + \bar{\boldsymbol{q}}_{\boldsymbol{e}}^{\times})\right]\boldsymbol{\omega} &(68)\\ &= -\boldsymbol{\omega}^T\boldsymbol{u} + k\bar{\boldsymbol{q}}_{\boldsymbol{e}}^T(1 + \bar{\boldsymbol{q}}_{\boldsymbol{e}}^{\times})\boldsymbol{\omega} &(69)\\ &= -\boldsymbol{\omega}^T(\boldsymbol{u} - k\bar{\boldsymbol{q}}_{\boldsymbol{e}}) &(70)\end{aligned}$$

Substituting feedback control law $\boldsymbol{u} = P\boldsymbol{\omega} + k\bar{\boldsymbol{q}}_{\boldsymbol{e}}$ with $P > 0$ into Eq. (70), we have

$$\dot{V} = -\boldsymbol{\omega}^T P\boldsymbol{\omega} < 0. \tag{71}$$

Therefore, Eq. (71) attains the Lyapunov stability. The control law is given by

$$\boldsymbol{u} = P\boldsymbol{\omega} + k\bar{\boldsymbol{q}}_{\boldsymbol{e}}, \quad P > 0, \quad k > 0. \tag{72}$$

APPENDIX B: VERTICES

When considering attitude control of a spacecraft with a DGVSCMG, the number of scheduling parameters can be always set to three. Therefore, the number of vertices can be taken $2^3 = 8$. The number of scheduling parameters are 3 with $2^3 = 8$ vertices. Let $\rho_{i\min}$ and $\rho_{i\max}$ denote the lower and the upper bound of ρ_i. Using these parameters and introducing the following interpolation parameters $\alpha_{i\min}$ and $\alpha_{i\max}$, the scheduling parameters ρ_i can be described as follows:

$$\rho_i = \alpha_{i\min}\rho_{i\min} + \alpha_{i\max}\rho_{i\max}, \quad 0 \leq \alpha_{i\min}, \alpha_{i\max} \leq 1, \quad \alpha_{i\min} + \alpha_{i\max} = 1 \tag{73}$$

Then, the convex combination coefficients $\lambda_i(\boldsymbol{\rho})$ are calculated as in Table 3. The range of the scheduling parameters are given as in Table 4.

Table 3. Convex combination coefficients $\lambda_i(\boldsymbol{\rho})$.

i	$\boldsymbol{\rho}$	$\lambda_i(\boldsymbol{\rho})$	binary
1	$[\rho_{1\min}, \rho_{2\min}, \rho_{3\min}]^T$	$\alpha_{1\min}\alpha_{2\min}\alpha_{3\min}$	000
2	$[\rho_{1\min}, \rho_{2\min}, \rho_{3\max}]^T$	$\alpha_{1\min}\alpha_{2\min}\alpha_{3\max}$	001
3	$[\rho_{1\min}, \rho_{2\max}, \rho_{3\min}]^T$	$\alpha_{1\min}\alpha_{2\max}\alpha_{3\min}$	010
4	$[\rho_{1\min}, \rho_{2\max}, \rho_{3\max}]^T$	$\alpha_{1\min}\alpha_{2\max}\alpha_{3\max}$	011
5	$[\rho_{1\max}, \rho_{2\min}, \rho_{3\min}]^T$	$\alpha_{1\max}\alpha_{2\min}\alpha_{3\min}$	100
6	$[\rho_{1\max}, \rho_{2\min}, \rho_{3\max}]^T$	$\alpha_{1\max}\alpha_{2\min}\alpha_{3\max}$	101
7	$[\rho_{1\max}, \rho_{2\max}, \rho_{3\min}]^T$	$\alpha_{1\max}\alpha_{2\max}\alpha_{3\min}$	110
8	$[\rho_{1\max}, \rho_{2\max}, \rho_{3\max}]^T$	$\alpha_{1\max}\alpha_{2\max}\alpha_{3\max}$	111

Table 4. Range of the scheduling parameters.

variable	min[rad/s]	max[rad/s]
ρ_1	-700	700
ρ_2	-700	700
ρ_3	-700	700

REFERENCES

[1] Wie, B.: Singularity Escape/Avoidance Steering Logic for Control Moment Gyro Systems, *Journal of Guidance, Control, and Dynamics*, Vol. 28, No. 5, 2005, pp. 948-956.

[2] Kurokawa, H.: Survey of Theory and Steering Laws of Single-Gimbal Control Moment Gyros, *Journal of Guidance, Control, and Dynamics*, Vol. 30, No. 5, September-October 2007

[3] Ford, K. A. and Hall, C. D.: Singular Direction Avoidance Steering for Control Moment Gyros, *Journal of Guidance, Control, and Dynamics*, Vol. 23, No. 4, 2000, pp. 648-656.

[4] Okubo, H. and Tani, Y.: Singularity Robust Steering of Redundant Single Gimbal Control Moment Gyros for Small Satellites, *Proc. of the 8th International Symposium on Artificial Intelligence, Robotics and Automation in Space*, Munich, Germany, 2005, pp. 1-8.

[5] Marshall, A. and Tsiotras, P.: Spacecraft Angular Velocity Stabilization Using a Single-Gimbal Variable Speed Control Moment Gyro, *AIAA Paper 03-5654*, 2003.

[6] Yamada, K., Takatsuka, N., and Shima, T.: Spacecraft Pointing Control Using a Variable-Speed Control Moment Gyro, *Proc. of the 26th International Symposium on Space Technology and Science 2008-d-15*, 2008.

[7] Yoon, H. and Tsiotras, P.: Singularity Analysis of Variable-Speed Control Moment Gyros,*Journal of Guidance, Control, and Dynamics*, Vol. 27, No. 3, May-June 2004

[8] Ahmed, J. and Bernstein, D.: Adaptive Control of Double-Gimbal Control-Moment Gyro with Unbalanced Rotor, *Journal of Guidance, Control, and Dynamics*, Vol. 25, No. 1, January-February 2002

[9] Stevenson, D. and Schaub, H.: Nonlinear Control Analysis of a Double-Gimbal Variable-Speed Control Moment Gyroscope,*Journal of Guidance, Control, and Dynamics*, Vol. 35, No. 3, May-June 2012

[10] Fujii, K., Yamada, K., and Nakashima, H.: Spacecraft Attitude Control Using a Variable-Speed Double-Gimbal Control Moment Gyro, ISTS, 2013

[11] Sakuramata, N.: Attitude Control of a Spacecraft equipped with a DGVSCMG based on LPV modeling, Bachelor Thesis, Department of Aerospace Engineering, Osaka Prefecture University, Japan, 2011. (in Japanese)

[12] Sasaki, T., Sakuramata, N, and Shimomura, T.: Attitude Control of A Spacecraft with A DGVSCMG via LPV Control Theory, 56th Joint Automatic Control Conference, 2013. (in Japanese)

[13] Yoon, H. and Tsiotras, P.: Spacecraft Line-of-Sight Control Using a Single Variable-Speed Control Moment Gyro, *Journal of Guidance, Control, and Dynamics*, Vol. 29, No. 6, 2006, pp. 1295-1308.

[14] Tsiotras, P.: Stabilization and Optimality Results for the Attitude Control Problem, *Journal of Guidance, Control, and Dynamics*, Vol. 19, No. 4, July–August, 1996

[15] Apkarian, P., Gahinet, P., and Becker, G.: Self-Scheduled $\mathcal{H}_\infty$ Control of Linear Parameter-Varying Systems: A Design Example, *Automatica*, Vol. 31, No. 9, 1995, pp. 1251-1261.

[16] Shimomura, T. and Kubotani, T.: Gain-Scheduled Control under Common Lyapunov Functions: Conservatism Revisited, *Proc. of 2005 American Control Conference*, 2005, pp. 870-875.

[17] Kwon, S., Shimomura, T., and Okubo, H.: Pointing control of spacecraft using two SGCMGs via LPV modeling theory, *Acta Astronautica*, Vol. 68, 2011, pp. 1168–1175.

[18] Yamamoto, Y. and Shimomura, T.: Attitude Control of Spacecraft with VSCMGs using LPV Modeling Technique, *SICE Annual Conference*, August, Tokyo, Japan, 2011, pp. 1676–1681.

[19] Yamamoto, Y. and Shimomura, T. : Attitude Control of Spacecraft through A Simple LPV Model with A Virtual State Variable, *AIAA Guidance, Navigation, and Control Conference*, AIAA 2012-5005.